FEBRUARY 21 2023

Phase-modulated Rice model for statistical distributions of complex signals

D. Keith Wilson ; Vladimir E. Ostashev ; Max E. Krackow

Check for updates

J. Acoust. Soc. Am. 153, 1241–1256 (2023)
https://doi.org/10.1121/10.0017251

View Online
Export Citation
CrossMark

Related Content

Blood clot characterization by ultrasound Nakagami imaging

J Acoust Soc Am (April 2012)

Feasibility of using Nakagami distribution in evaluating the formation of ultrasound-induced thermal lesions

J. Acoust. Soc. Am. (June 2012)

Estimation of the Nakagami parameter from log-compressed ultrasonic backscattered envelopes (L)

J Acoust Soc Am (July 2003)

01 October 2023 09:00:47

Take the Lead in Acoustics

The ability to account for coupled physics phenomena lets you predict, optimize, and virtually test a design under real-world conditions – even before a first prototype is built.

» Learn more about COMSOL Multiphysics®

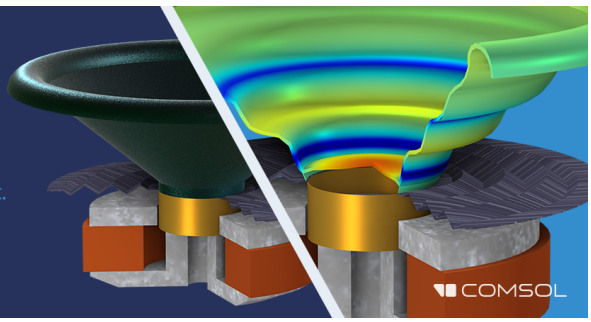

JASA ARTICLE

Phase-modulated Rice model for statistical distributions of complex signals

D. Keith Wilson,[a] Vladimir E. Ostashev, and Max E. Krackow
U.S. Army Engineer Research and Development Center, 72 Lyme Road, Hanover, New Hampshire 03755, USA

ABSTRACT:
The basic Rice model is commonly used to describe complex signal statistics from randomly scattered waves. It correctly describes weak (Born) scattering, as well as fully saturated scattering, and smoothly interpolates between these extremes. However, the basic Rice model is unsuitable for situations involving scattering by random inhomogeneities spanning a broad range of spatial scales, as commonly occurs for sound scattering by turbulence in the atmospheric boundary layer and other scenarios. In such scenarios, the phase variations are often considerably stronger than those predicted by the basic Rice model. Therefore, the basic Rice model is extended to include a random modulation in the signal phase, which is attributable to the influence of the largest, most energetic inhomogeneities in the propagation medium. Various joint and marginal distributions for the complex signal statistics are derived to incorporate the phase-modulation effect. Approximations of the phase-modulated Rice model involving the Nakagami distribution for amplitude, and the wrapped normal and von Mises distributions for phase, are also developed and analyzed. The phase-modulated Rice model and various approximations are shown to greatly improve agreement with simulated data for sound propagation in the near-ground atmosphere.
https://doi.org/10.1121/10.0017251

(Received 6 October 2022; revised 26 December 2022; accepted 28 January 2023; published online 21 February 2023)

[Editor: Philippe Blanc-Benon] Pages: 1241–1256

01 October 2023 09:00:47

I. INTRODUCTION

The amplitude and phase of acoustic signals fluctuate due to wave scattering by turbulence and other random processes in the atmosphere (see, for example, Refs. 1 and 2, and references therein). Statistical distributions of these fluctuations are important for many contemporary applications such as source detection probabilities, outdoor noise regulation, and auralization of flying aircraft.[3–6] In fact, the importance of signal amplitude and phase fluctuations in scattered waves extends to many fields besides atmospheric acoustics, including radio-wave propagation,[7–9] optics,[10,11] and ocean acoustics.[12–14] As a result, many physics-based and empirical statistical models have been proposed. Although amplitude statistics have received the bulk of attention, phase statistics can be important from the perspective of beamforming, passive ranging, travel-time tomography, and other applications.

This article is motivated by a particular shortcoming in current models for signal phase statistics. Specifically, experimental data for acoustic signals transmitted through the near-ground atmosphere often exhibit large phase variances relative to the log-amplitude variances.[15–18] When samples of the complex signal are plotted, this behavior leads to characteristic "arc" and "donut" shapes with few samples near the origin, indicating the near absence of large fading events in which the signal amplitude approaches zero. It is evident, for example, in Figs. 10 and 11 of Norris *et al.*,[15] Fig. 14 (the *exception* being 1000 Hz at 450 m downwind) and Fig. 15 (at 1000 Hz, except at 100 m upwind) of Cheinet *et al.*,[16] and Fig. 9 of Kamrath *et al.*[17] (the *exceptions* being at 3400 Hz, for 130 m on 09/25 at 06:45, for 130 m on 09/25 at 12:45, and for 39 m and 130 m on 09/27 at 12:48). Previously available models for complex signals, particularly the widely used Rice distribution (which describes a signal having normally distributed real and imaginary parts of equal variance and a non-zero deterministic mean),[12,13,19] do not correctly reproduce this signal behavior.

To address this problem, a new joint amplitude-phase distribution is proposed in this article, termed the *phase-modulated Rice model*. In this approach, the basic (unmodulated) Rice model is used for scattering by relatively small, Fresnel-zone scale turbulent eddies, which impact both signal amplitude and phase. Then, the phase of the "mean" signal in the basic Rice model is modulated with a von Mises distribution. This enhanced phase modulation is associated with relatively strong, large-scale turbulent eddies, which strongly impact the signal phase but not the amplitude.

Conceptually, this approach bears some similarity to that of Mamyshev and Odintsov,[20] who partition the phase variations for acoustic signals scattered in the atmosphere into "local" and "turbulent" contributions (the authors' usage of these terms might be roughly interpreted to mean "quasi-deterministic" and "random," respectively). However, in the present formulation, we view both contributions as resulting from atmospheric turbulence, although at different spatial scales as distinguished by the size of the Fresnel zone.

[a]Electronic mail: d.keith.wilson@usace.army.mil

This article is organized as follows. In Sec. II A, the basic Rice model is described and some significant results for the phase distribution are derived and compared to other models. With this foundation, we introduce the phase-modulated Rice model, for which the joint and marginal probability density functions (pdfs) of amplitude and phase are formulated in Sec. II B. Since applications often involve explicit characterization of the real and imaginary parts of the complex signal, those distributions are derived as well, in Sec. II C. Next, in Sec. III, comparisons are made with simulations for sound propagation in the near-ground atmosphere, including scattering by turbulence, refraction, and ground reflections. Section IV summarizes the results. The Appendix provides additional analytical results based on approximating the phase-modulated Rice model with a Nakagami pdf for amplitude and wrapped normal pdf for phase.

II. PHASE-MODULATED RICE DISTRIBUTION

A. Basic Rice model and approximations

The Rice distribution, which is widely used in both electromagnetics and acoustics,[6,8,10,21] applies to weakly scattered signals consisting of a deterministic contribution plus many randomly scattered contributions modeled based on the Born (single scattering) approximation. It is also valid in the limit of fully saturated scattering (fully randomized scattering with a vanishing deterministic mean), and furthermore interpolates smoothly between the extremes of weak scattering and full saturation. These features help to explain its popularity.

In this article, we will use the terminology *Rice model* to refer to a statistical process for a complex signal with normally distributed real and imaginary parts. *Rice distribution* will refer specifically to the amplitude pdf derived from the Rice model.

Let us designate the complex signal as $Z = X + iY = Ae^{i\Phi}$, where X and Y are random variables for the real and imaginary parts of the signal, $A = |Z| = \sqrt{X^2 + Y^2}$ is the random amplitude, and Φ is the random phase. By convention, we take the angular interval to be $-\pi < \Phi \leq \pi$. The signal power (squared amplitude) is $S = A^2 = X^2 + Y^2$. For the Rice model, the means of X and Y are, in general, non-zero. We thus write $X \sim \mathcal{N}(\nu_x, \sigma^2)$ and $Y \sim \mathcal{N}(\nu_y, \sigma^2)$, where $\mathcal{N}(\nu, \sigma^2)$ indicates a normal pdf with mean ν and variance σ^2. Furthermore, $\nu_x = \nu\cos\theta$, $\nu_y = \nu\sin\theta$, where $\nu = \sqrt{\nu_x^2 + \nu_y^2}$ is the amplitude of the mean signal and θ is the phase angle of the mean signal. Hence $X = \nu_x + \sigma n_x$ and $Y = \nu_y + \sigma n_y$, where n_x and n_y are independent, zero-mean normal random variables with unit variance. Note that the mean power is $\langle S\rangle = \langle X^2\rangle + \langle Y^2\rangle = \nu_x^2 + \sigma^2\langle n_x^2\rangle + \nu_y^2 + \sigma^2\langle n_y^2\rangle = \nu^2 + 2\sigma^2$. If we normalize the power to have a mean of 1, then $\nu^2 + 2\sigma^2 = 1$, and hence $\nu^2 = 1 - 2\sigma^2$. The Rice model is sometimes written in other forms by defining the *Rice factor* $K = \nu^2/2\sigma^2$, which is a ratio of the power in the steady part of the signal divided by the power in the varying part. When the mean is set to 1, the other parameters can be regarded as depending only on K, namely, $\nu^2 = K/(K+1)$ and $2\sigma^2 = 1/(K+1)$.

Based on the definitions of X and Y as independent normal random variables, their joint pdf is

$$f_{XY}(x, y|\nu, \theta, \sigma^2) = \frac{1}{2\pi\sigma^2}\exp\left(-\frac{(x-\nu_x)^2 + (y-\nu_y)^2}{2\sigma^2}\right). \quad (1)$$

In this article, we follow the convention of indicating random variables in upper case, and functional arguments related to those variables in lower case. From Eq. (1), we find the joint pdf for the amplitude A and phase Φ by setting $f_{A\Phi}(a, \phi) = [|J_{a,\phi}(x, y)|f_{XY}(x, y)]_{a,\phi}$, where $J_{a,\phi}(x, y) = a$ is the Jacobian. The result is

$$f_{A\Phi}(a, \phi|\nu, \theta, \sigma^2) = \frac{a}{2\pi\sigma^2}\exp\left(-\frac{a^2 + \nu^2}{2\sigma^2}\right)\exp\left(\frac{a\tilde{\nu}}{\sigma^2}\right), \quad (2)$$

where $\tilde{\nu} = \nu_x\cos\phi + \nu_y\sin\phi = \nu(\cos\theta\cos\phi + \sin\theta\sin\phi) = \nu\cos(\phi - \theta)$. Note that A and Φ are *not* independent in the Rice model because the second exponential in the preceding equation cannot be factored into separate functions of a and $\tilde{\nu}$.

The pdf of amplitude for the Rice model (simply called the *Rice distribution*) is obtained by marginalizing (integrating) the joint pdf, Eq. (2), over the phase. The result is

$$f_A(a|\nu, \sigma^2) = \frac{a}{\sigma^2}\exp\left(-\frac{a^2 + \nu^2}{2\sigma^2}\right)I_0\left(\frac{a\nu}{\sigma^2}\right). \quad (3)$$

Here, I_0 is the modified Bessel function of the first kind, order zero. In the limit of full saturation, $\nu \to 0$, the Rice pdf reduces to the Rayleigh pdf, $f_R(a|\sigma^2) = (a/\sigma^2)\exp(-a^2/2\sigma^2)$.

The power (amplitude squared) distribution for the Rice model is obtained by setting $f_S(s) = [|da/ds|f_A(a)]_s$, with $s = a^2$, leading to

$$f_S(s|\nu, \sigma^2) = \frac{1}{2\sigma^2}\exp\left(-\frac{s + \nu^2}{2\sigma^2}\right)I_0\left(\frac{\nu\sqrt{s}}{\sigma^2}\right). \quad (4)$$

This equation is an order 2, noncentral Erlang distribution.[6] The variance of this distribution is $4\sigma^2(\sigma^2 + \nu^2)$. When the distribution is normalized to unit mean, the variance depends only on K and is given by $(2K+1)/(K+1)^2$. The variance of the normalized power is equivalent to the scintillation index, which is usually defined in the literature as $S_I^2 = \langle s^2\rangle/\langle s\rangle^2 - 1 = \langle(s - \langle s\rangle)^2\rangle/\langle s\rangle^2$. This quantity equals 1 for $K = 0$ and decreases monotonically as K increases. Thus, the basic Rice model does not predict super scintillation, i.e., $S_I^2 > 1$. (An approach to including super scintillation in the Rice model, as attributable to modulation of the signal intensity by turbulent intermittency, is discussed in Ref. 21. This intensity modulation could potentially be combined with the phase modulation considered in this article to create a more comprehensive statistical model.)

01 October 2023 09:00:47

https://doi.org/10.1121/10.0017251

Equation (4), normalized to unit mean, is plotted for $K=0$, 1, 4, and 16 in Fig. 1. For $K=0$, the distribution is exponential. As K is increased, it becomes more peaked around the mean.

For comparison, also plotted in Fig. 1 is the gamma distribution. The gamma distribution for signal power transforms to the Nakagami pdf for signal amplitude[23] [Eq. (A2) in the Appendix], which is widely used in the communications literature. The gamma pdf is given by

$$f_\Gamma(s|k,b) = \frac{s^{k-1}}{\Gamma(k)b^k}\exp\left(-\frac{s}{b}\right), \tag{5}$$

where k is the shape parameter and b is the scale parameter. The mean and variance of the gamma distribution are kb and kb^2, respectively. The scintillation index equals $1/k$. For full saturation conditions, the gamma pdf, like the Rice model, predicts an exponential pdf for power. However, unlike the Rice model, which is consistent with the Born approximation for weak scattering, the gamma pdf is justifiable for scattering regimes other than full saturation only from an empirical perspective. The gamma pdfs plotted in Fig. 1 correspond to setting the mean to 1 and the variance to the same value as in the corresponding Rice pdf, i.e., $k=(K+1)^2/(2K+1)$. The corresponding values of k are 1 (for $K=0$), 1.33 (for $K=1$), 2.78 (for $K=4$), and 8.76 (for $K=16$). The two pdfs agree well for small and large K, but differ somewhat for moderate values, particularly with regard to the frequency of deep fading (events with S near zero).

The phase distribution for the Rice model is obtained by marginalizing Eq. (2) over amplitude. The resulting integral can be solved using Eq. (3.462.5) from Ref. [22], and written in the following form,[24] which depends only on K (rather than ν and σ^2 individually):

$$f_\Phi(\phi|K,\theta) = \frac{1}{2\pi}e^{-K}\Big[1+\sqrt{K\pi}\cos(\phi-\theta)\exp\big(K\cos^2(\phi-\theta)\big)\mathrm{erfc}\Big(-\sqrt{K}\cos(\phi-\theta)\Big)\Big]. \tag{6}$$

Here, $\mathrm{erfc}(x)$ is the complementary error function. Equation (6) is plotted in Fig. 2 for $K=0$, 1, 4, and 16, and $\theta=0$. When $K=0$, the phase is uniformly distributed since there is no mean component. As K is increased, the phase becomes more strongly peaked around θ.

It is of interest to compare the Rice phase distribution to other common distributions for angular variables. In particular, the *wrapped normal* and *von Mises* distributions are widely used. Although moments for angular variables can be defined in the familiar way, alternative definitions accounting for the cyclical nature of these variables are typically employed. In particular, the nth circular moment is defined as $m_n = \langle e^{in\Phi}\rangle$. The *circular mean* is thus $m_1 = \langle e^{i\Phi}\rangle$. The *circular variance* is defined as $1-R$, where $R=|m_1|$. Because the Rice phase distribution is an even function and $m_1>0$ when $\theta=0$, we have $m_1 = \langle\cos\phi\rangle = R$. While it does not appear possible to calculate $\langle\cos\phi\rangle$ analytically, it can be readily done by multiplying $f_\Phi(\phi|K,0)$ from Eq. (6) by $\cos\phi$ and numerically integrating between $-\pi$ and π.

First let us consider the wrapped normal pdf, defined as

$$f_{\mathrm{WN}}(\theta|\sigma_u^2) = \frac{1}{\sqrt{2\pi}\,\sigma_u}\sum_{n=-\infty}^{\infty}\exp\left[-\frac{(\theta+2\pi n)^2}{2\sigma_u^2}\right], \tag{7}$$

where σ_u^2 indicates the unwrapped phase variance. The wrapped normal distribution provides a smooth transition between weak scattering ($\sigma_u^2 \ll 1$), for which the phase is normally distributed, and full saturation ($\sigma_u^2 \gg 1$), for which the phase is uniformly distributed. The circular moments of the wrapped normal distribution are $m_n = \exp(-n^2\sigma_u^2/2)$.[25]

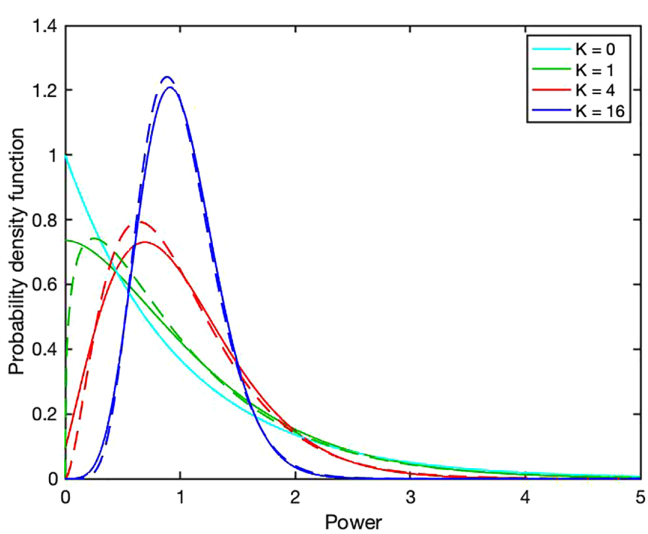

FIG. 1. (Color online) Probability density functions (pdfs) for signal power according to the Rice model, for various values of the Rice factor K (solid lines). The dashed lines correspond to gamma pdfs when the power variance is matched to the Rice phase pdf, as described in the text.

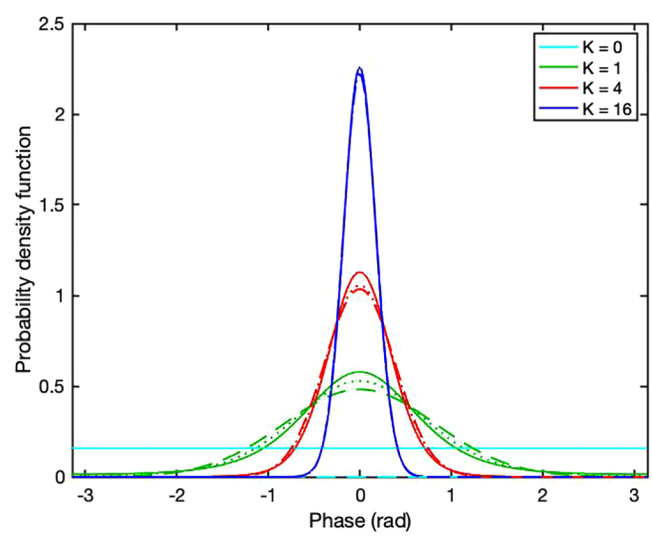

FIG. 2. (Color online) Probability density functions for signal phase according to the Rice model, for various values of the Rice factor K (solid lines). The dashed and dotted lines correspond to the wrapped normal and von Mises pdfs, respectively, when the circular variance is matched to the Rice phase pdf.

01 October 2023 09:00:47

The circular variance is thus $1 - \exp(-\sigma_u^2/2)$. Next, consider the von Mises pdf, defined as

$$f_{\mathrm{VM}}(\theta|\kappa) = \frac{1}{2\pi I_0(\kappa)} \exp(\kappa \cos\theta). \tag{8}$$

Here, κ is a measure of concentration: the larger the value of κ, the smaller the variance. The circular moments of the von Mises distribution are $m_n = I_{|n|}(\kappa)/I_0(\kappa)$,[25] where I_n is the nth-order modified Bessel function of the first kind. The circular variance of the von Mises distribution is thus $1 - I_1(\kappa)/I_0(\kappa)$.

Figure 3 plots the parameters σ_u^2 in the wrapped normal distribution and κ in the von Mises distribution, as determined by matching the circular variances of these distributions to the Rice phase distribution as a function of K. In particular, the value of R in the Rice distribution is determined numerically by trapezoidal integration for each K. Then, for the wrapped normal distribution, σ_u^2 is set to $-2\ln R$. For the von Mises distribution, κ is found such that $I_1(\kappa)/I_0(\kappa) = R$.

The wrapped normal and von Mises distributions, with circular variances thus matched, are compared to the Rice phase distribution in Fig. 2. The corresponding values of the circular variance are 1 (for $K = 0$), 0.290 (for $K = 1$), 0.072 (for $K = 4$), and 0.016 (for $K = 16$). Clearly, the three distributions approximate each other closely. Agreement is best for small and large K, but deviates more noticeably for moderate values.

Based on results thus far, the pdf for signal power in the Rice model can be reasonably approximated with a gamma pdf (and the pdf for signal amplitude by a Nakagami pdf), whereas the pdf for signal phase can be reasonably approximated with a wrapped normal or a von Mises pdf. In fact, a recent analysis[26] indicates excellent agreement between experimental data for sound scattering in the atmosphere and a model combining the Nakagami and wrapped normal pdfs. However, some care should be taken with *ad hoc*, independent combinations of amplitude and phase distributions. As pointed out earlier, the amplitude and phase statistics predicted by the Rice model are dependent. This dependence is physically significant; for example, the phase variance is intrinsically large when a signal amplitude is fully saturated. However, mathematically, a Nakagami pdf characteristic of a saturated signal can be readily combined with a phase pdf exhibiting small variance. Some efforts have been made to construct consistent models for complex signals by extending a Nakagami pdf for the amplitude to also include phase.[27,28] However, those models do not appear applicable in the context of random wave scattering as considered in this article.

Figure 4 shows the joint pdf of the real and imaginary parts according to the Rice model [Eq. (1)]. Figure 5 shows the corresponding joint pdf based on assuming that the amplitude and phase are independent, with the amplitude given by a Nakagami pdf and the phase by a wrapped normal pdf [Eq. (A9)]. As before, the shape parameter in the Nakagami pdf is chosen such that the power variance matches the Rice model, and the variance parameter in the wrapped normal pdf is chosen such that the circular variance matches the Rice model. Subplots for Rice factors of $K = 0$, $K = 1$, $K = 4$ and $K = 16$ are shown. For $K = 0$, the models coincide. When $K > 0$, in comparison to the Rice model the Nakagami/wrapped normal pdfs are noticeably flattened on the side of the meshes for negative real part.

B. Random phase modulation

Sound propagation in the atmospheric boundary layer (ABL) is influenced by turbulent eddies across a broad range

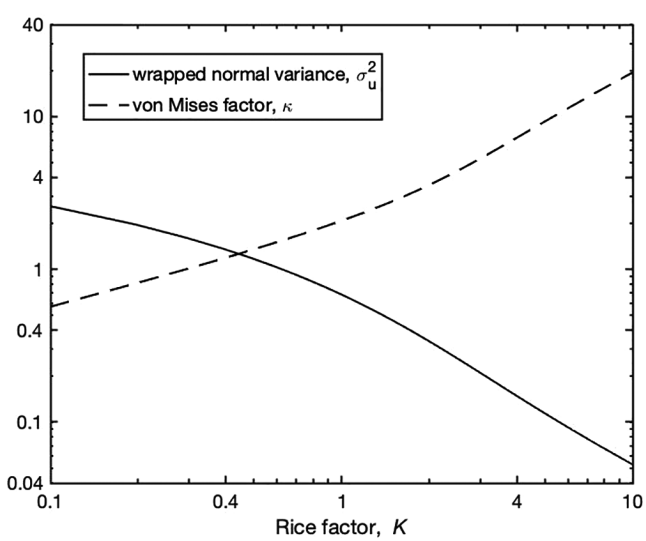

FIG. 3. Variance parameter σ_u^2 for the wrapped normal distribution (solid line) and dispersion parameter κ from the von Mises distribution (dashed line) as a function of the Rice factor K, as determined by matching the circular variances in the distributions, as described in the text.

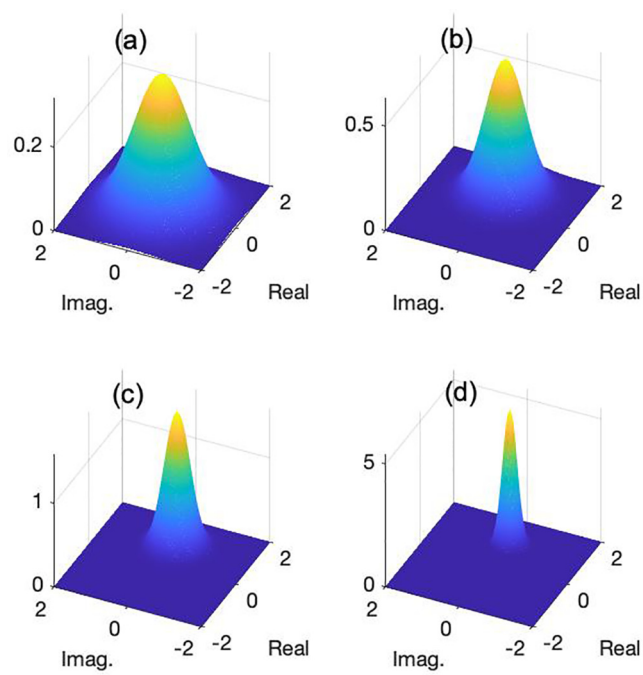

FIG. 4. (Color online) Joint pdf for the real and imaginary parts of a complex signal according to the unmodulated Rice model. The mean power is normalized to one and the mean phase is zero. Each subplot is for a particular value of the Rice factor K. (a) $K = 0$. (b) $K = 1$. (c) $K = 4$. (d) $K = 16$.

01 October 2023 09:00:47

https://doi.org/10.1121/10.0017251

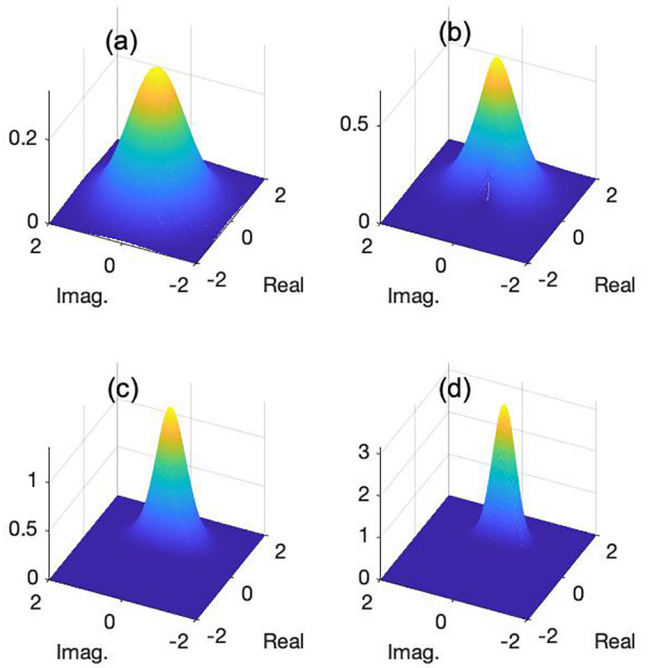

FIG. 5. (Color online) Joint pdf for the real and imaginary parts of a complex signal according to a model assuming independent amplitude and phase, with the power (squared amplitude) given by a gamma pdf and the phase by a wrapped normal pdf. The shape parameter in the gamma pdf is chosen such that the power variance matches the Rice model. The variance parameter in the wrapped normal pdf is chosen such that the circular variance matches the Rice model. The mean power is normalized to one and the mean phase is zero. Each subplot is for a particular value of the Rice factor K. (a) $K=0$. (b) $K=1$. (c) $K=4$. (d) $K=16$.

of spatial scales, from centimeters to kilometers.[1] Particularly in conditions of weak scattering [defined as situations where the log-amplitude, $\chi = \ln(A/A_0)$, in which A_0 is the unscattered amplitude, has a variance such that $\langle \chi^2 \rangle \ll 1$; see, for example, the discussion in Ref. 29], the amplitude fluctuations are caused by relatively small-scale turbulent eddies with sizes on the order of the Fresnel zone, whereas phase fluctuations are strongly impacted by the largest, most energetic eddies. As a result, the phase variance is often much larger than the log-amplitude variance. The Rice model, as described in Sec. II A, does not capture the relatively large phase variance induced by the large-scale turbulent eddies.

To address this problem, one possible modeling approach is to view $f_{A\Phi}(a,\phi|\nu,\theta,\sigma^2)$, Eq. (2), as the pdf for sound scattering by the small-scale (Fresnel-zone size) turbulence only. Phase fluctuations due to large-scale eddies can then be included by varying (modulating) the phase angle θ randomly over a relatively long time scale. This concept is depicted in Fig. 6. The various colors represent samples collected over a relatively short time window, for which the basic (unmodulated) Rice model provides a reasonable description of the scattering statistics. Over these short time windows, signal samples appear as circular "clouds" of points offset at a fixed amplitude from the origin. The phase modulation taking place over relatively long time scales sweeps the clouds around an arc or the entire unit circle.

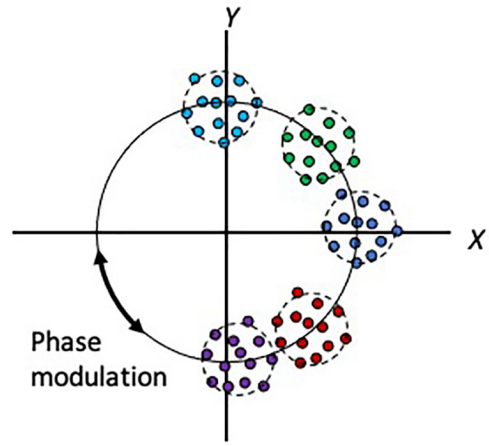

FIG. 6. (Color online) Conceptual depiction of the phase-modulated Rice distribution. The various colors represent samples collected over a relatively short time window, during which the basic Rice model is applicable. The modulation varies the mean angle (as defined over the short time window) along the unit circle over a relatively longer time scale.

Mathematically, we describe the large-scale phase modulation with a pdf $f_\Theta(\theta|\gamma_\theta)$, where γ_θ represents one or more statistical parameters upon which Θ depends. Based on this approach, a compound (integral) pdf is formulated for the overall process as

$$f_{A\Phi}(a,\phi|\nu,\sigma^2,\gamma_\theta) = \int f_{A\Phi}(a,\phi|\nu,\theta,\sigma^2) f_\Theta(\theta|\gamma_\theta)\, d\theta, \qquad (9)$$

where Θ is the randomized phase angle averaged over the long time scale. Note that the phase modulation impacts only the phase statistics; it does not impact the amplitude statistics because Eq. (3) is independent of θ. Thus, the mean power of the phase-modulated Rice distribution is given by $\nu^2 + 2\sigma^2$, as before.

The wrapped normal and von Mises distributions are both reasonable candidates for $f_\Theta(\theta|\gamma_\theta)$. For the former, we set $f_\Theta(\theta|\gamma_\theta) = f_{\mathrm{WN}}(\theta|\sigma_\theta^2)$, where σ_θ^2 is the unwrapped phase variance due to the large-scale variations. We then find by substituting Eqs. (2) and (7) into Eq. (9),

$$\begin{aligned} &f_{A\Phi}(a,\phi|\nu,\sigma^2,\sigma_\theta^2) \\ &\quad = \frac{a}{(2\pi)^{3/2}\sigma^2\sigma_\theta} \exp\left(-\frac{a^2+\nu^2}{2\sigma^2}\right) \\ &\qquad \times \sum_{n=-\infty}^{\infty} \int_{-\pi}^{\pi} \exp\left(\frac{a\tilde{\nu}}{\sigma^2}\right) \exp\left[-\frac{(\theta+2\pi n)^2}{2\sigma_\theta^2}\right] d\theta. \qquad (10) \end{aligned}$$

One potential advantage of this approach is that since the Rice phase pdf is approximately normal, the overall phase pdf should be well approximated by a wrapped normal pdf with unwrapped variance $\sigma_\theta^2 + \sigma_u^2$, where σ_u^2 is the small-scale phase variance obtained by matching the circular variances of the Rice and unwrapped normal pdfs, as described in Sec. II A. This hypothesis will be examined later. A disadvantage of Eq. (10) is that neither the integral nor the sum can be evaluated analytically, which complicates subsequent analysis. Some approximate analytical results for the wrapped normal phase

01 October 2023 09:00:47

distribution, based on assuming that the signal amplitude follows a Nakagami distribution, are provided in the Appendix.

Alternatively, we can use the von Mises pdf for $f_\Theta(\theta|\gamma_\theta)$. Substituting Eqs. (2) and (8) into Eq. (9) leads to

$$f_{A\Phi}(a,\phi|\nu,\sigma^2,\kappa) = \frac{a}{4\pi^2\sigma^2 I_0(\kappa)}\exp\left(-\frac{a^2+\nu^2}{2\sigma^2}\right) \times \int_{-\pi}^{\pi}\exp\left[\frac{a\nu}{\sigma^2}\cos(\phi-\theta) + \kappa\cos\theta\right]d\theta. \quad (11)$$

This result can be recast as

$$f_{A\Phi}(a,\phi|\nu,\sigma^2,\kappa) = \frac{a}{4\pi^2\sigma^2 I_0(\kappa)}\exp\left(-\frac{a^2+\nu^2}{2\sigma^2}\right) \times \int_{-\pi}^{\pi}\exp\left[\left(\kappa+\frac{a\nu\cos\phi}{\sigma^2}\right)\cos\theta + \frac{a\nu\sin\phi}{\sigma^2}\sin\theta\right]d\theta. \quad (12)$$

Introducing the angle α, where $\tan\alpha = a\nu\sin\phi/(\kappa\sigma^2 + a\nu\cos\phi)$, we obtain

$$f_{A\Phi}(a,\phi|\nu,\sigma^2,\kappa) = \frac{a}{4\pi^2\sigma^2 I_0(\kappa)}\exp\left(-\frac{a^2+\nu^2}{2\sigma^2}\right) \times \int_{-\pi}^{\pi}\exp\left[\sqrt{\kappa^2+\frac{2\kappa\nu a\cos\phi}{\sigma^2}+\frac{\nu^2a^2}{\sigma^4}} \times\sin(\theta-\alpha)\right]d\theta. \quad (13)$$

Recognizing the integral over θ as the modified Bessel function of the first kind I_0 results in

$$f_{A\Phi}(a,\phi|\nu,\sigma^2,\kappa) = \frac{a}{2\pi\sigma^2 I_0(\kappa)}\exp\left(-\frac{a^2+\nu^2}{2\sigma^2}\right) \times I_0\left(\sqrt{\kappa^2+\frac{2\kappa\nu a\cos\phi}{\sigma^2}+\frac{\nu^2a^2}{\sigma^4}}\right). \quad (14)$$

This formula gives the phase-modulated Rice distribution when the modulation is modeled with the von Mises pdf. Its simplicity relative to Eq. (10) for the wrapped normal pdf facilitates calculations of the distributions for the phase fluctuations and real and imaginary parts of the complex signal.

We obtain the joint distribution of the real and imaginary parts of the complex signal from Eq. (14) using the relationship $f_{XY}(x,y) = f_{A\Phi}(a,\phi)[|J_{x,y}(a,\phi)|]_{a,\phi}$, where $J_{x,y}(a,\phi) = 1/a$ is the Jacobian. The result is

$$f_{XY}(x,y|\nu,\sigma^2,\kappa) = \frac{\exp\left(-\frac{x^2+y^2+\nu^2}{2\sigma^2}\right)}{2\pi\sigma^2 I_0(\kappa)} \times I_0\left(\sqrt{\kappa^2+\frac{2\kappa\nu x}{\sigma^2}+\frac{\nu^2(x^2+y^2)}{\sigma^4}}\right). \quad (15)$$

Figure 7 shows joint pdfs for the Rice model with phase modulation from the von Mises pdf [Eq. (15)]. Shown are results for $K=4$ and $K=16$, with $\kappa=0.5$ and $\kappa=4$. (Unlike in Fig. 4, small values of K are not shown because the phase is already close to uniform for those cases, so the modulation has little impact.) We see that the phase-modulated Rice model is able to qualitatively reproduce cases such as those in Fig. 9 of Ref. 17 involving large phase variances. This behavior cannot be reproduced with the unmodulated Rice model.

We can obtain the amplitude and phase distributions by marginalizing Eq. (14). As mentioned earlier, the phase modulation does not impact amplitude, and therefore the amplitude pdf coincides with Eq. (3). The phase pdf is obtained by marginalizing the joint pdf, Eq. (14), over amplitude, with the result

$$f_\Phi(\phi|\nu,\sigma^2,\kappa) = \int_0^\infty f_{A\Phi}(a,\phi|\nu,\sigma^2,\kappa)\,da = \frac{\exp\left(-\frac{\nu^2}{2\sigma^2}\right)}{2\pi\sigma^2 I_0(\kappa)}\int_0^\infty a e^{-(a^2/2\sigma^2)} \times I_0\left(\sqrt{\kappa^2+\frac{2\kappa\nu a\cos\phi}{\sigma^2}+\frac{\nu^2a^2}{\sigma^4}}\right)da. \quad (16)$$

Making the substitution $\bar{a} = a/\nu$ (valid for $\nu \neq 0$), the equation can be written as a function of K and κ only,

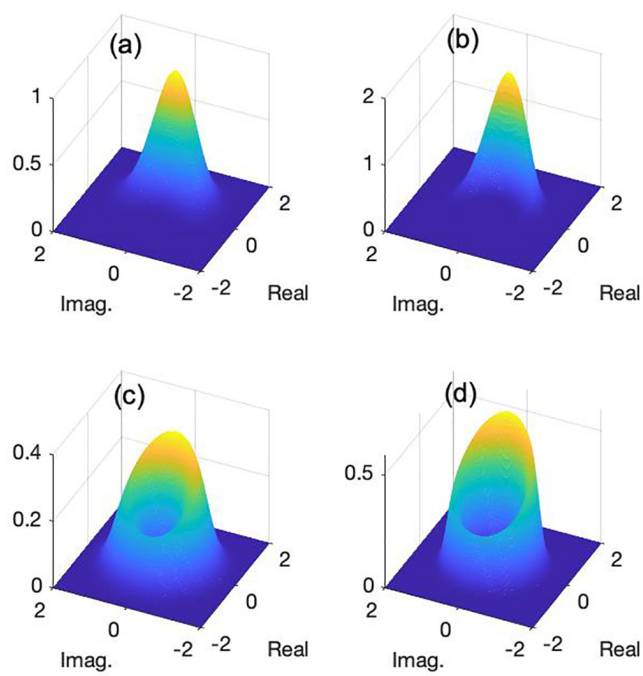

FIG. 7. (Color online) Joint pdf for the real and imaginary parts of a complex signal according to the Rice model with phase modulated by a von Mises pdf. The mean power is normalized to one and the mean phase is zero. Each subplot is for a different combination of the Rice factor K and the von Mises factor κ. (a) $K=4$ and $\kappa=4$. (b) $K=16$ and $\kappa=4$. (c) $K=4$ and $\kappa=0.5$. (d) $K=16$ and $\kappa=0.5$.

01 October 2023 09:00:47

https://doi.org/10.1121/10.0017251

$$f_\Phi(\phi|K,\kappa) = \frac{K\exp(-K)}{\pi I_0(\kappa)}\int_0^\infty \bar{a}e^{-K\bar{a}^2} I_0\left(\sqrt{\kappa^2+4\kappa K\bar{a}\cos\phi+4K^2\bar{a}^2}\right)d\bar{a}. \tag{17}$$

It follows from this equation that $f_\Phi(\phi|K,\kappa)$ is an even function of ϕ so that the mean value $\langle\phi\rangle = 0$. In the limit $K \to 0$, it can be shown that $f_\Phi(\phi|K,\kappa) \to 1/(2\pi)$, as should be the case for fully saturated scattering since the phase modulation can have no impact when the phase distribution is already uniform.

Figure 8 shows probability density functions for the signal phase obtained by numerically integrating Eq. (17) by the trapezoidal rule. The Rice factor K is set to 4, and four values of κ are shown: ∞, 8, 2, and 0.5. Note that $\kappa = \infty$ corresponds to the unmodulated case as plotted in Fig. 2 while decreasing κ corresponds to increasing phase modulation. It is readily apparent that the phase pdf becomes more nearly uniform as κ is decreased to small values. Also, shown in the figure are approximations with wrapped normal pdfs. For these curves (the dashed lines), the total unwrapped phase variance was set to the sum of contributions from the ordinary Rice model and the phase-modulation process, i.e., to $\sigma_\theta^2 + \sigma_u^2$, as suggested earlier in this section. The value of σ_u^2 was determined from the circular variance of the Rice distribution as described in Sec. II A, whereas σ_θ^2 was chosen such that the circular variances for the large-scale phase modulation would match the von Mises pdf, i.e., $\sigma_\theta^2 = -2\ln[I_1(\kappa)/I_0(\kappa)]$. The wrapped normal pdf is seen to provide an excellent approximation, as it did in the unmodulated case.

C. Real and imaginary parts

In this subsection, we consider statistics of the real and imaginary parts of the complex signal. The means and

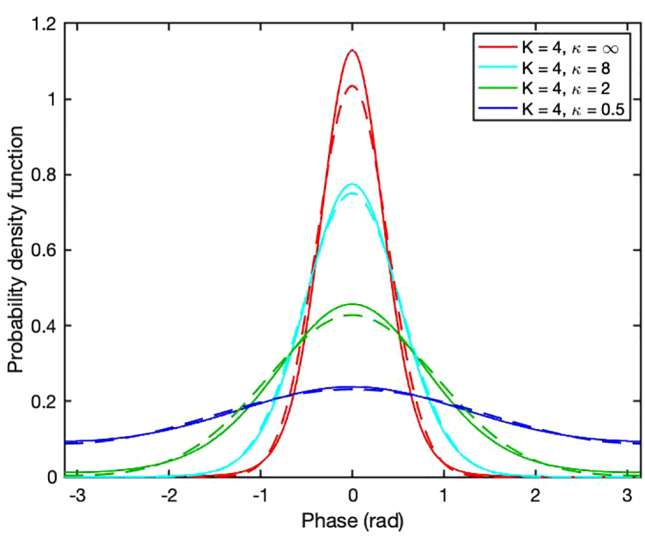

FIG. 8. (Color online) Probability density functions for signal phase according to the Rice model with von Mises phase modulation, for a Rice factor $K = 4$ and various values κ (solid lines). Also, shown are wrapped normal pdfs (dashed lines), for which the total unwrapped phase variance is set to the sum of contributions from the ordinary Rice model and the phase-modulation process, as described in the text.

variances readily follow from known properties of the wrapped normal and von Mises distributions.

As discussed earlier, in the phase-modulated Rice model, the real and imaginary parts are given by $X = \nu\cos\Theta + \sigma n_x$ and $Y = \nu\sin\Theta + \sigma n_y$, where n_x and n_y are independent, zero-mean normal random variables with unit variance, ν is the mean amplitude, and Θ is the phase angle for the modulating distribution. Hence, for the means we have $\langle X\rangle = \nu\langle\cos\Theta\rangle$ and $\langle Y\rangle = \nu\langle\sin\Theta\rangle$. For the variances, $\sigma_x^2 = \langle X^2\rangle - \langle X\rangle^2 = \nu^2(\langle\cos^2\Theta\rangle - \langle\cos\Theta\rangle^2) + \sigma^2$ and $\sigma_y^2 = \langle Y^2\rangle - \langle Y\rangle^2 = \nu^2(\langle\sin^2\Theta\rangle - \langle\sin\Theta\rangle^2) + \sigma^2$. Applying trigonometric identities results in $\sigma_x^2 = (\nu^2/2)(1 + \langle\cos(2\Theta)\rangle - 2\langle\cos\Theta\rangle^2) + \sigma^2$ and $\sigma_y^2 = (\nu^2/2)(1 - \langle\cos(2\Theta)\rangle - 2\langle\sin\Theta\rangle^2) + \sigma^2$.

The expected values of the trigonometric functions can be readily determined from the circular moments. As mentioned earlier, for the wrapped normal distribution, $m_n = \langle\exp(in\Theta)\rangle = \exp(-n^2\sigma_\theta^2/2)$. Hence $\langle\cos\Theta\rangle = \exp(-\sigma_\theta^2/2)$, $\langle\sin\Theta\rangle = 0$, and $\langle\cos(2\Theta)\rangle = \exp(-2\sigma_\theta^2)$. We thus have

$$\langle X\rangle = \nu e^{-\sigma_\theta^2/2}, \tag{18}$$

$$\langle Y\rangle = 0, \tag{19}$$

$$\sigma_x^2 = \frac{\nu^2}{2}\left(1 + e^{-2\sigma_\theta^2} - 2e^{-\sigma_\theta^2}\right) + \sigma^2, \tag{20}$$

and

$$\sigma_y^2 = \frac{\nu^2}{2}\left(1 - e^{-2\sigma_\theta^2}\right) + \sigma^2. \tag{21}$$

For the ratio of the variances of the imaginary part to the real part, which is a measure of the anisotropy of the joint distribution, we have

$$\frac{\sigma_y^2}{\sigma_x^2} = \frac{K(1 - e^{-2\sigma_\theta^2}) + 1}{K(1 - 2e^{-\sigma_\theta^2} + e^{-2\sigma_\theta^2}) + 1}. \tag{22}$$

Figure 9 shows the ratio σ_y^2/σ_x^2 as a function of K and σ_θ/π. When $K \to 0$, i.e., fully saturated scattering, the variances of the real and imaginary parts are always approximately equal regardless of the phase modulation. The variance ratio is also close to 1 when $\sigma_\theta \approx 0$ or when $\sigma_\theta \gg 1$. In the former case, there is no phase modulation, so the Rice distribution has equal real and imaginary parts. In the latter case, the phase modulation wraps around the unit circle, and thus the real and imaginary parts have similar pdfs (although the phasor diagram may look like a "donut" when the Rice parameter is small). The ratio peaks when K is relatively large and σ_θ is small but non-zero. This regime corresponds to an arc of points on the phasor diagram, with relatively large phase variance and small log-amplitude variance.

Let us next consider the case where Θ follows a von Mises distribution. Then $m_n = \langle\exp(in\Theta)\rangle = I_n(\kappa)/I_0(\kappa)$, and we find for the means and variances

$$\langle X\rangle = \nu\langle\cos(\Theta)\rangle + \sigma\langle n_x\rangle = \frac{\nu I_1(\kappa)}{I_0(\kappa)}, \tag{23}$$

01 October 2023 09:00:47

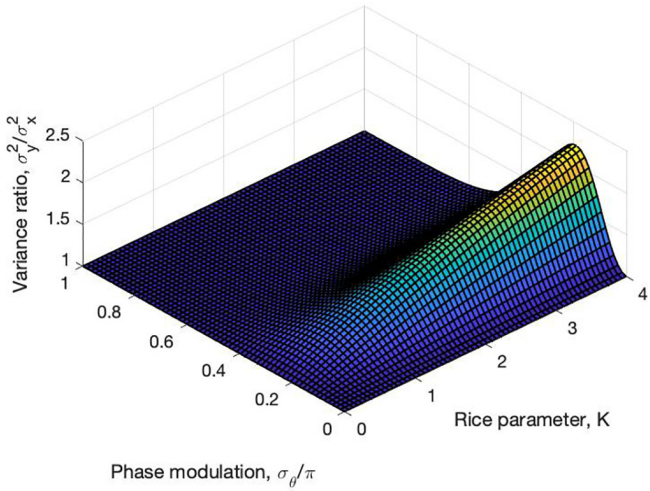

FIG. 9. (Color online) Variance ratio σ_y^2/σ_x^2 for the Rice model with phase modulation from a wrapped normal distribution. The ratio is plotted as a function of the Rice parameter K and phase modulation standard deviation σ_θ.

$$\langle Y\rangle = \nu\langle \sin(\Theta)\rangle + \sigma\langle n_y\rangle = 0, \tag{24}$$

$$\sigma_x^2 = \frac{\nu^2}{2}\left[1 - \frac{2I_1^2(\kappa)}{I_0^2(\kappa)} + \frac{I_2(\kappa)}{I_0(\kappa)}\right] + \sigma^2, \tag{25}$$

and

$$\sigma_y^2 = \frac{\nu^2}{2}\left[1 - \frac{I_2(\kappa)}{I_0(\kappa)}\right] + \sigma^2. \tag{26}$$

Next, consider the full distributions for the real and imaginary parts of the complex signal as based upon the phase-modulated Rice model. These are found by marginalizing the joint pdf $f_{XY}(x,y)$, i.e.,

$$f_X(x) = \int_{-\infty}^{\infty} f_{XY}(x,y)\,dy \tag{27}$$

and

$$f_Y(y) = \int_{-\infty}^{\infty} f_{XY}(x,y)\,dx. \tag{28}$$

Substituting Eq. (15) into Eq. (27), we obtain the pdf for the real part as

$$f_X(x|\nu,\sigma^2,\kappa) = \frac{\exp\left(-\frac{\nu^2+x^2}{2\sigma^2}\right)}{\pi\sigma^2 I_0(\kappa)} \times \int_0^{\infty} e^{-y^2/2\sigma^2} I_0\left(\sqrt{\kappa^2 + \frac{2\kappa\nu x}{\sigma^2} + \frac{\nu^2(x^2+y^2)}{\sigma^4}}\right) dy. \tag{29}$$

Here, we took into account that the integrand is an even function of y. Similarly, we obtain the distribution for the imaginary part as

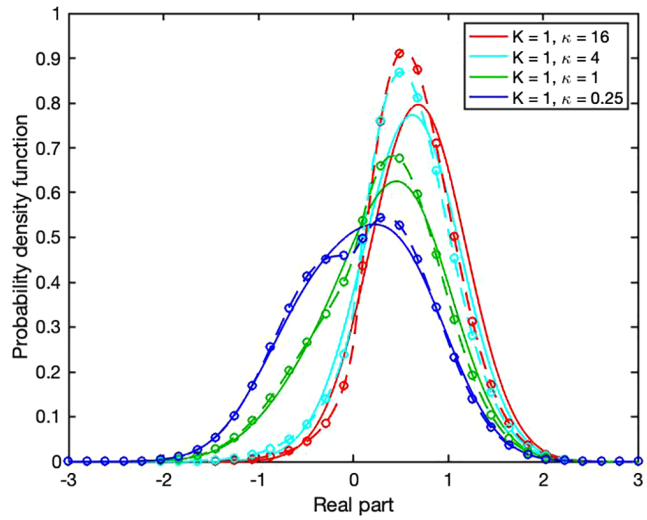

FIG. 10. (Color online) Probability density functions for the real component, for the phase-modulated Rice model with a Rice factor $K=1$ and various values of the von Mises parameter κ (solid lines). The mean power is normalized to 1. The dashed lines correspond to the combined model with a Nakagami pdf for the amplitude and wrapped normal pdf for the phase, with the circular variance matched to the phase-modulated Rice model. The circles are the analytical approximation to the Nakagami/wrapped normal model given by Eq. (A14).

$$f_Y(y|\nu,\sigma^2,\kappa) = \frac{\exp\left(-\frac{\nu^2+y^2}{2\sigma^2}\right)}{2\pi\sigma^2 I_0(\kappa)} \times \int_{-\infty}^{\infty} e^{-x^2/2\sigma^2} I_0\left(\sqrt{\kappa^2 + \frac{2\kappa\nu x}{\sigma^2} + \frac{\nu^2(x^2+y^2)}{\sigma^4}}\right) dx. \tag{30}$$

While the integrals in Eqs. (29) and (30) cannot be evaluated analytically, they can readily be evaluated numerically. Figures 10 and 11 depict the distribution for the real part as calculated by numerical integration of Eq. (29) by the trapezoidal rule, for $K=1$ and $K=4$, respectively.

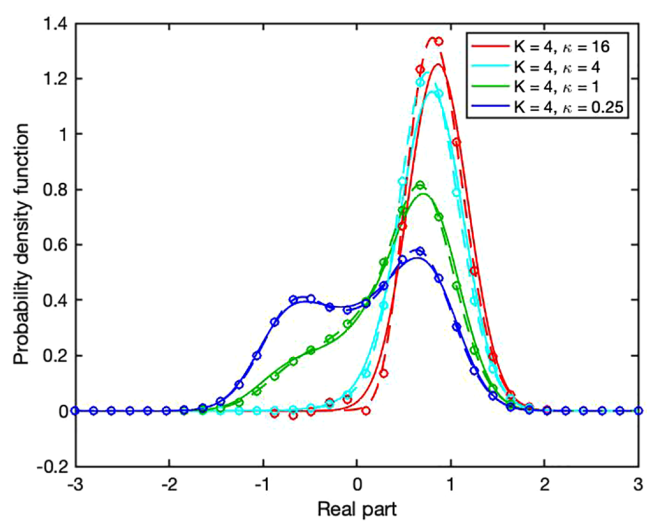

FIG. 11. (Color online) Same as Fig. 10, except for $K=4$.

01 October 2023 09:00:47

https://doi.org/10.1121/10.0017251

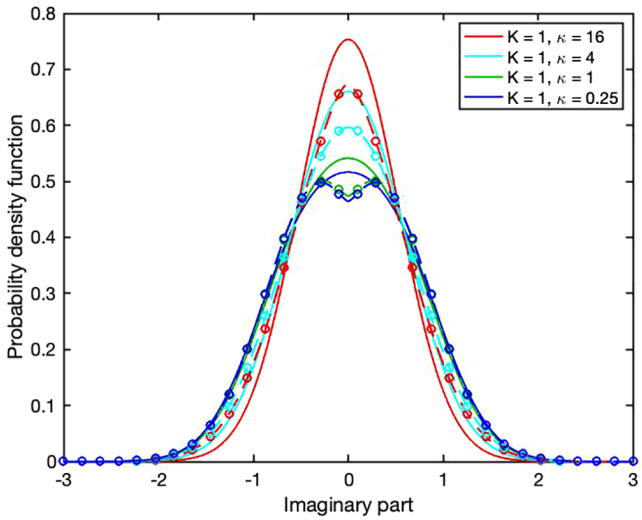

FIG. 12. (Color online) Probability density functions for the imaginary component, for the phase-modulated Rice model with a Rice factor $K = 1$ and various values of the von Mises parameter κ (solid lines). The mean power is normalized to 1. The dashed lines correspond to the combined model with a Nakagami pdf for the amplitude and wrapped normal pdf for the phase, with the circular variance matched to the phase-modulated Rice model. The circles are the analytical approximation to the Nakagami/wrapped normal model given by Eq. (A6).

The mean power is normalized to 1. The four solid lines correspond to $\kappa = 1/4$, 1, 4, and 16. For relatively large values of K and κ, the real part has a well-defined peak around $x = 1$. As κ is decreased, the peak broadens, and ultimately the distribution becomes bimodal.

Figures 12 and 13 are the same as Figs. 10 and 11, except that they show the distribution for the imaginary part as calculated by numerical integration of Eq. (30). For relatively large values of K and κ, the imaginary part has a well-defined peak around $y = 0$. As with the real part, as κ is decreased, the peak broadens and ultimately becomes bimodal.

The dashed lines and circles in Figs. 10–13 correspond to the combined model with a Nakagami pdf for the amplitude and wrapped normal pdf for the phase, with the circular variance matched to the phase-modulated Rice model. The circles are based on a Fourier series approximation as willl be discussed in the Appendix.

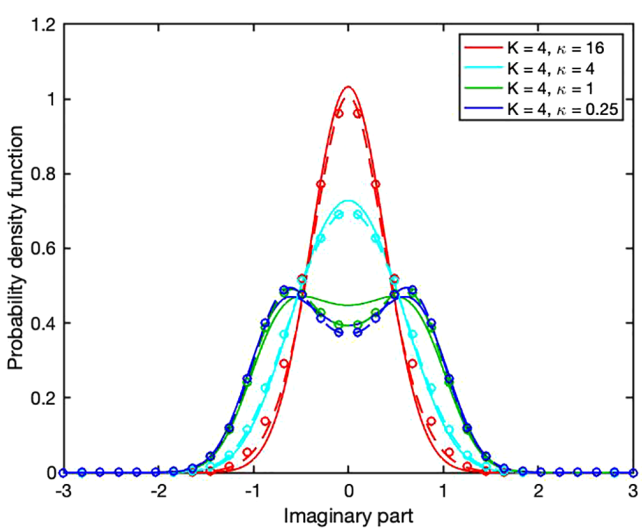

FIG. 13. (Color online) Same as Fig. 12, except for $K = 4$.

III. COMPARISON TO SIMULATIONS

This section compares the phase-modulated Rice model to numerical simulations of sound propagation in the atmosphere. The simulations realistically represent interactions of sound with the ground surface, refraction by the vertical wind and temperature profiles, and scattering by atmospheric turbulence across a wide range of spatial scales. The propagation calculations were performed with a narrow-angle Crank-Nicholson parabolic equation (PE);[1,30] such PEs are widely used for acoustic and radio-wave propagation in the atmosphere and ocean. The primary benefit of the simulation approach is that it enables the creation of large, controlled datasets in a manner that would be practically impossible with actual outdoor experiments. Of course, not all complexities of the real atmosphere can be captured; in particular, the simulations assume flat, homogeneous ground and steady-state atmospheric forcings.

The simulation methodology used in this article was employed previously to study the impacts of refraction and scattering on the signal power distribution.[31] The reader is referred to that article for a more detailed description of the approach. Reference 31 also focused on various forms of the gamma distribution for the purpose of addressing propagation uncertainties; the Rice distribution was not considered. In this article, we employ the simulations to characterize statistics of the full complex signal, including phase.

The simulations employ similarity theory to model the vertical profiles of wind and temperature, and the atmospheric turbulence spectrum. In particular, the profiles are modeled with the Monin-Obukhov similarity theory (MOST), which describes the profiles with four parameters: (1) the friction velocity, u_* (proportional to the wind shear), (2) the sensible heat flux from the surface to the overlying air, Q_H, (3) the height from the surface, z, and (4) the Boussinesq buoyancy parameter $\beta = g/T_s$, where g is the gravitational acceleration and T_s the surface temperature in Kelvin. The profile equations employed in the present article are described fully in Sec. 2.2.3 of Ostashev and Wilson.[11] In the following calculations, we set $u_* = 0.6$ m/s and $Q_H = 100\,\mathrm{Wm}^{-2}$, as characteristic of windy, mostly cloudy conditions.

The turbulence is modeled with the von Kármán spectrum for the inertial and energy-containing subranges, as fully described by Kamrath *et al.*[17] Three separate contributions are added together. The first represents temperature fluctuations, the second shear-induced velocity fluctuations, and the third buoyancy-induced velocity fluctuations. The first two contributions obey MOST, with the length scales being approximately proportional to height. The third is derived from convective boundary-layer scaling, which employs Q_H, β, and the boundary-layer inversion height, z_i,

01 October 2023 09:00:47

with the length scale being proportional to z_i. Here, we set $z_i = 1000$ m. Because MOST has height-dependent parameters, the inhomogeneous spectral method described in Sec. 9.1.2 of Ref. 1 is used to synthesize the random turbulent fluctuations for input to the PE.

For all of the PE calculations, the source and receiver heights were set to 5 m and 1.2 m, respectively. The maximum horizontal range is 1000 m, and the vertical extent of the domain is 100 m plus a 50-wavelength attenuating layer. (Beyond this range, signals are typically saturated at audible frequencies.) A relaxation model (Secs. 10.2.2–10.2.3 of Ref. 1) is used with parameters for loose soil.

The PE calculations of the complex signals were performed at 100, 200, and 400 Hz. For each of these frequencies, 4096 random realizations were performed in both the downwind and upwind directions. In the downwind direction, the positive wind gradient generally leads to ducting and multipath interference. In the upwind direction, a refractive shadow zone forms at a distance of about 200 m from the source, such that much of the sound energy reaching the receiver is randomly scattered by turbulence.

Figures 14–16 show the simulated joint pdfs for the real and imaginary parts of the complex signal at 100, 200, and 400 Hz, respectively. The phase angle was adjusted to zero mean. The top row in each figure shows downwind propagation at 250, 500, and 1000 m, whereas the bottom row is upwind propagation at 250, 500, and 1000 m. Although it is not possible to make direct comparisons, the simulated complex signals have a similar appearance, frequency, and range dependence to experimental studies of outdoor sound propagation.[15,16,18]

We describe the general appearance of the scatter plots with three informal categories, namely, "arc," "donut," and "disk" shapes. Figures 14(a) and 14(d) exemplify arcs, whereas Figs. 15(b) and 16(a) exemplify donuts. Figures 14(a) and 15(a) are transitional cases. The remaining figures exemplify disks. The arcs occur when there is a weak log-amplitude variance and a moderate phase variance (i.e., the standard deviation of the phase is smaller than 2π). The donuts also involve a weak log-amplitude variance, but with a phase variance large enough to span the unit circle, as occurs for fully saturated scattering. The disks have a large enough log-amplitude variance to fill the center. Note that cases with a disk displaced from the origin, as characteristic of the basic (unmodulated) Rice model, do not occur in this simulated dataset.

Figure 17 shows some illustrative marginal pdfs for the power (top row) and phase (bottom row) for these three cases. The first column is for an arc case, namely Fig. 14(a) (100 Hz in the downwind direction at a range of 250 m). The second column is for a donut case, namely Fig. 15(b) (200 Hz in the downwind direction at a range of 500 m). The third column is for a disk case, namely, Fig. 16(e) (400 Hz in the upwind direction at a range of 500 m). Essentially, Figs. 17(a) and 17(b) have similar power distributions, with a maximum at non-zero power, whereas Fig. 17(c) has an exponential pdf for power. On the other hand, Fig. 17(d) has a phase distribution with a well-defined peak at zero, whereas Figs. 17(e) and 17(f) exhibit uniformly distributed phase.

Also, shown in Fig. 17(a)–17(c) are fits to the simulated pdfs using two different models for the signal power,

01 October 2023 09:00:47

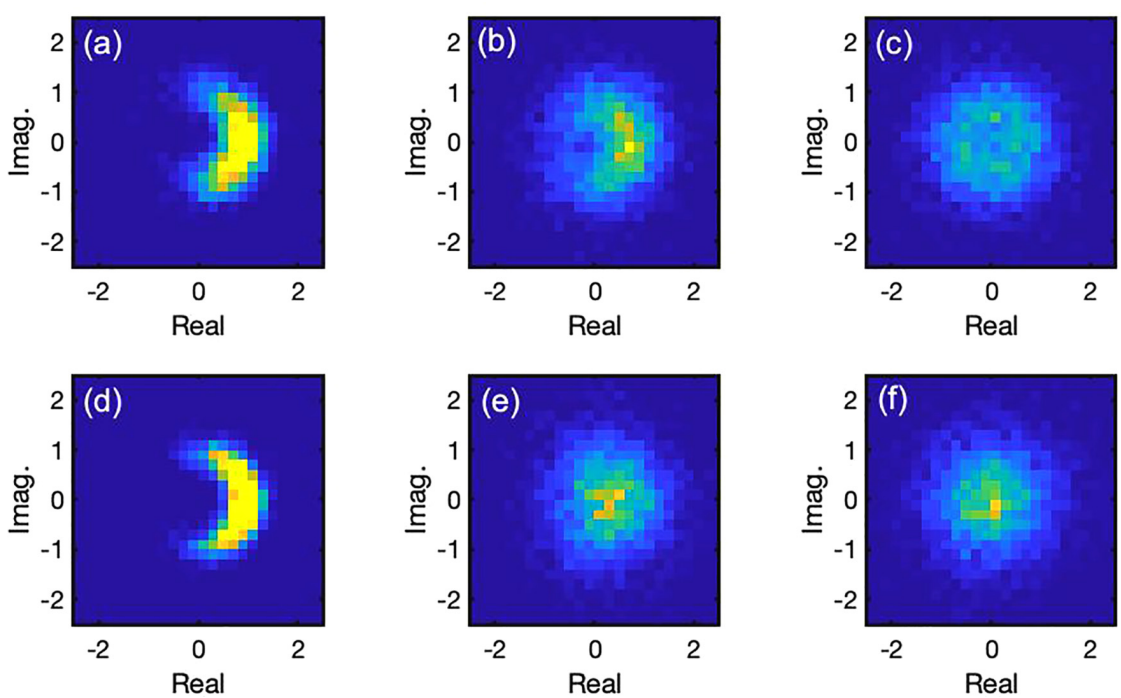

FIG. 14. (Color online) Joint pdf for the real and imaginary parts of the simulated signals at 100 Hz. Top row is downwind at ranges of (a) 250 m, (b) 500 m, and (c) 1000 m. Bottom row is upwind at ranges of (d) 250 m, (e) 500 m, and (f) 1000 m. Coloration represents probability density on a scale range from 0 (dark blue) to 0.5 (bright yellow).

https://doi.org/10.1121/10.0017251

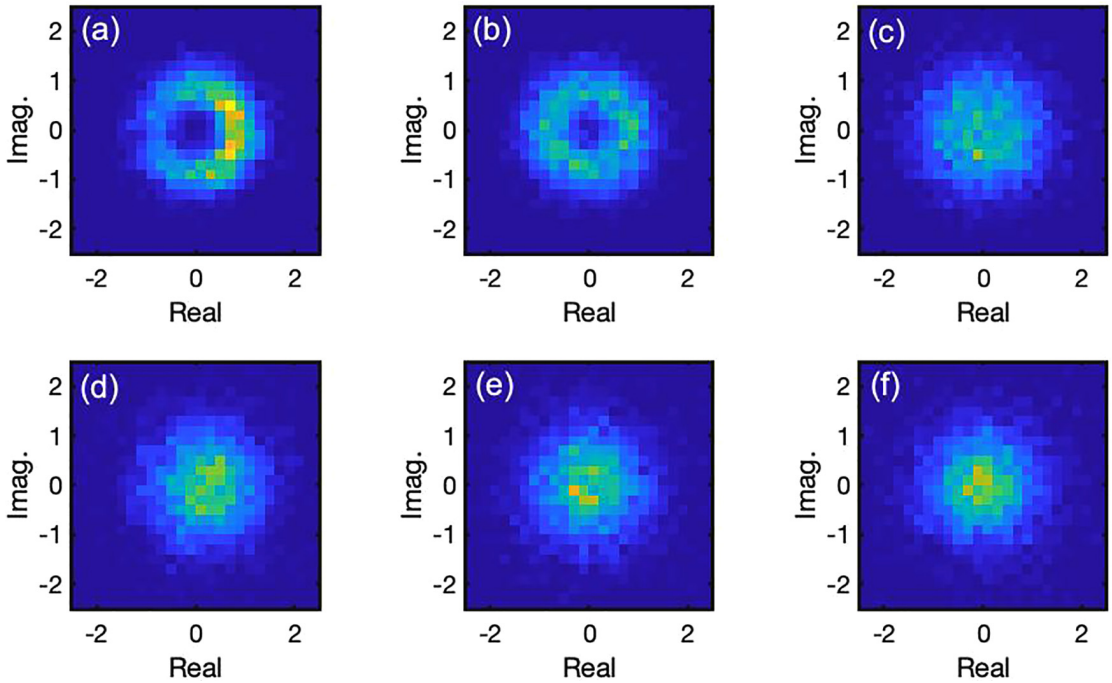

FIG. 15. (Color online) Same as Fig. 14, except for 200 Hz.

namely the Rice [more precisely, the order 2, noncentral Erlang, Eq. (4)] and gamma [Eq. (5)] distributions. The pdf parameters (K and k, respectively) were determined from the simulated values of S_I^2. Figures 17(d)–17(f) show fits to the simulated pdfs for the signal phase, namely the phase-modulated Rice [Eq. (17)] and wrapped-normal [Eq. (7)] distributions. For the former, κ was determined from the simulated values of the circular variance after first determining K from S_I^2. For the latter, σ_u^2 follows from the equation for the circular variance, $1 - \exp(-\sigma_u^2/2)$. Even with these rather simple fitting procedures, the models provide excellent agreement with the simulations.

Figure 18(a) shows Rice factors K as determined from the scintillation indices (normalized power variances) of the simulation data. As derived in Sec. II A for the Rice model, with or without phase modulation, $S_I^2 = (2K+1)/(K+1)^2$.

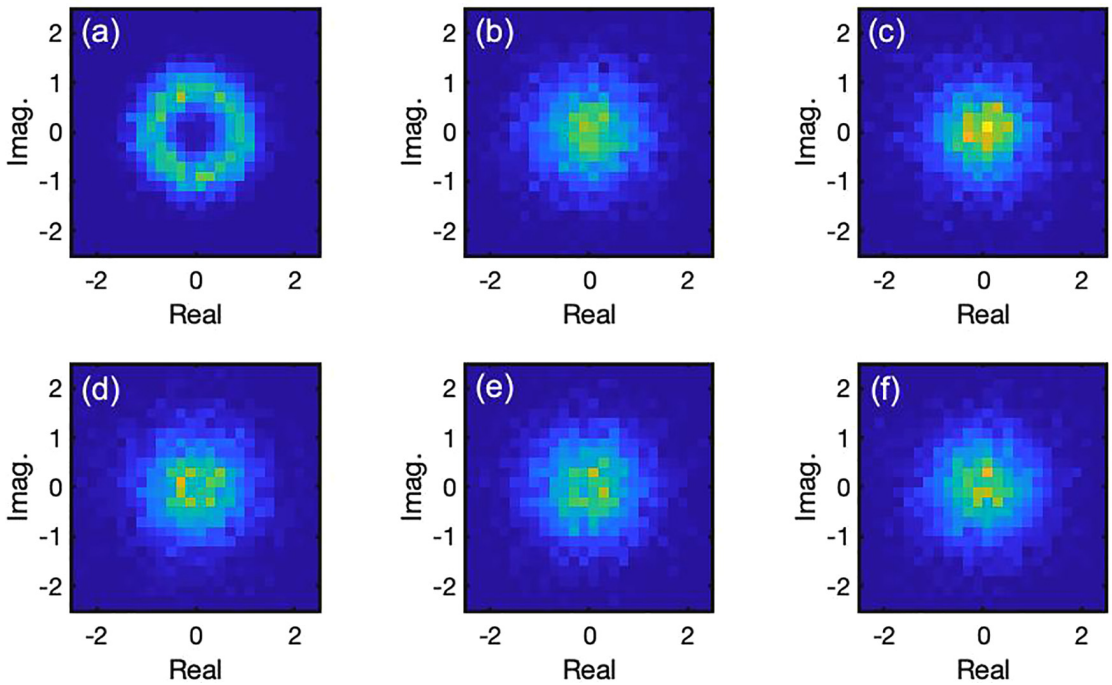

FIG. 16. (Color online) Same as Fig. 14, except for 400 Hz.

01 October 2023 09:00:47

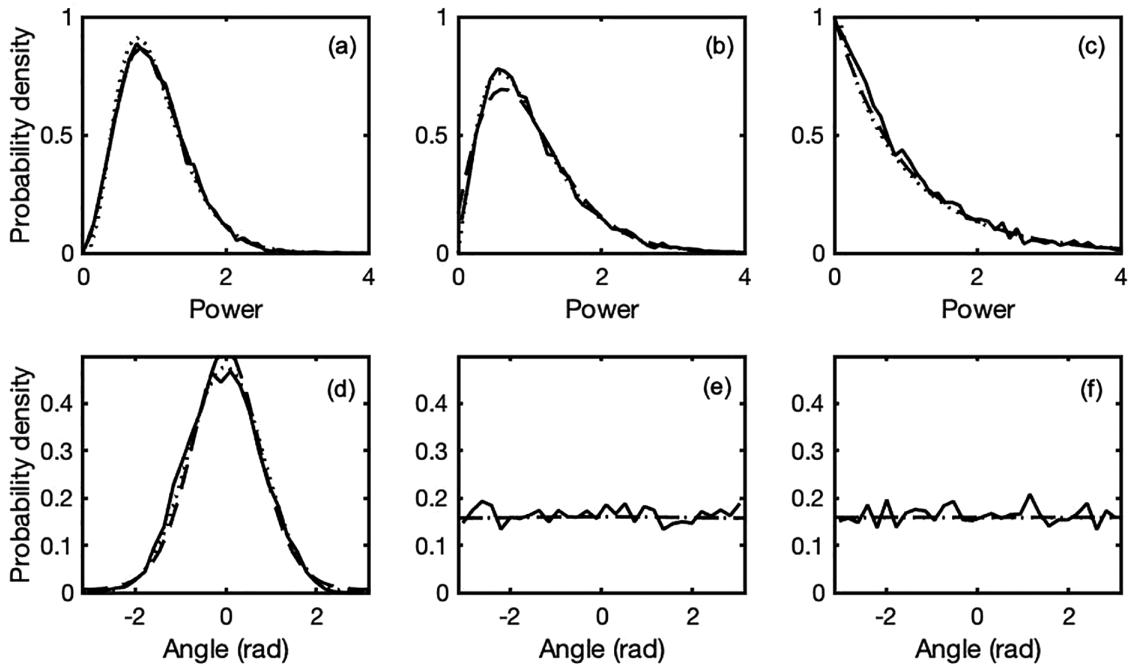

FIG. 17. Illustrative pdfs for the signal power (top row) and phase (bottom row). The first column (a and d) is for 100 Hz, in the downwind direction at a range of 250 m. The second column (b and e) is for 200 Hz, in the downwind direction at a range of 500 m. The third column (c and f) is for 400 Hz, in the upwind direction at a range of 500 m. Simulation results are the solid lines. Also, shown in the top row are fitted distributions for the Rice (dashed lines) and gamma (dotted lines) models. Shown in the bottom row are fitted distributions for the phase-modulated Rice (dashed lines) and wrapped normal (dotted lines) models.

Solving this equation for positive K yields the values plotted in Fig. 18(a). Results are shown in the upwind and downwind directions. In the upwind direction, $K = 0$, as is indicative of full saturation, for all cases, except at the range 250 m at 100 Hz. In the downwind direction, K is between 5 and 7 at 250 m for all frequencies and decreases with range, particularly at 400 Hz. At the downwind ranges of 500 m and 750 m, K is actually larger at 200 than at 100 Hz. (The cause is uncertain, but is plausibly connected to the impedance ground boundary condition.) Overall, we observe that the phase modulation is most important in the downwind direction, particularly for low frequencies.

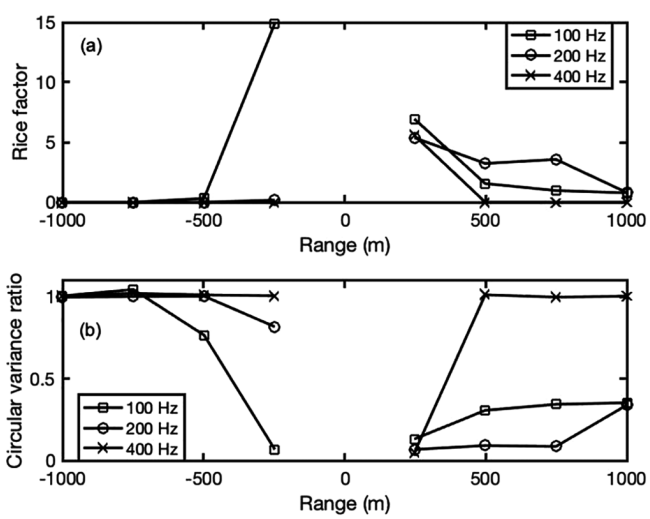

FIG. 18. (a) Rice factor K for amplitude distributions fitted to the simulation data. (b) Ratio of the circular variance as predicted by the unmodulated Rice model divided by the total circular variance in the simulation data. For both (a) and (b), results are shown for upwind and downwind propagation at ranges of 250 m, 500 m, 750 m, and 1000 m. Negative ranges are upwind; positive ranges are downwind. Squares are for 100 Hz, circles for 200 Hz, and x's for 400 Hz.

Figure 18(b) is the ratio of the circular variance as predicted for the unmodulated Rice model divided by the total circular variance in the simulation data. Recall from the discussion following Eq. (6) that this equation can be used to calculate the value of $\langle \cos \phi \rangle$, and hence the circular variance, associated with the unmodulated Rice model. Taking the ratio of this value to the actual circular variance from the simulations yields the values plotted in Fig. 18(b). A small value of this ratio indicates that the phase variance in the signal is driven primarily by the phase modulation process. A value near 1 indicates that the phase modulation is unimportant. Upwind, the phase modulation is most important nearer to the source and at lower frequencies. The same trend essentially holds downwind, although the phase modulation is considerably more important in this direction.

The Kullback-Leibler (KL) divergence[32] quantifies agreement between two pdfs. We use it here to assess the relative agreement between the simulation data and modeled pdfs. A relatively smaller value of the KL divergence indicates a better fit; the absolute values have no direct interpretation in the present context. Figure 19(a) shows the KL divergence between the simulated signal power and three model distributions: the exponential, gamma, and order-2 noncentral Erlang (Rice model). Figure 19(b) shows the KL divergence between the simulated signal power and the

01 October 2023 09:00:47

https://doi.org/10.1121/10.0017251

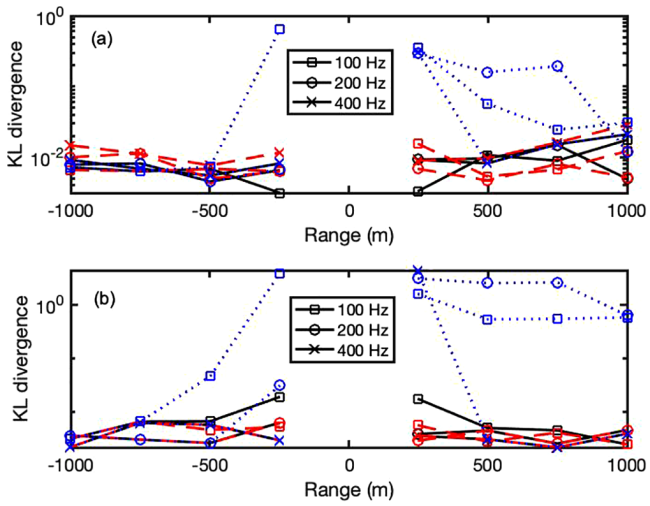

FIG. 19. (Color online) KL divergence between the simulation data and various model pdfs. (a) Divergence between the simulation data and the order 2, noncentral Erlang (black solid lines), gamma (red dashed lines), and exponential (blue dotted lines) distributions for signal power. (b) Divergence between the simulation data and the phase-modulated Rice (black solid lines), wrapped-normal (red dashed lines), and unmodulated Rice (blue dotted lines) distributions for signal phase. Negative ranges are upwind; positive ranges are downwind. Squares are for 100 Hz, circles for 200 Hz, and x's for 400 Hz.

wrapped-normal, unmodulated Rice, and phase-modulated Rice distributions for signal phase. As would be expected, the exponential pdf for power and the unmodulated Rice for phase provide reasonable results only for full saturation. There do not appear to be clear trends favoring the other models, except perhaps for 100 Hz at the 250 m range. In that case, the Rice model provides a somewhat better fit than the gamma for signal power in both the upwind and downwind directions, whereas the wrapped normal provides a better fit than the modulated Rice distribution for the phase. However, the discrepancies between these models are quite small, as evident from Figs. 14(a) and 14(d).

IV. CONCLUSIONS

In this article, the Rice model was extended by modulating the phase according to a von Mises distribution. This modulation was introduced to reproduce the relatively large phase variance characteristic of sound propagation in the atmosphere and other media, and is attributable to the impact of large-scale turbulence in the atmosphere. The phase modulation leads to excellent agreement with complex signal statistics for simulated sound propagation in the near-ground atmosphere. The simulations include many realistic complicating factors such as scattering by a broad turbulence spectrum, refraction by wind and temperature gradients, and reflections from an impedance ground surface. The phase modulation was shown to be particularly important for downwind propagation at relatively low frequencies and short distances.

The statistical process underlying the phase-modulated Rice model is straightforward, consisting of normally distributed fluctuations of the real and imaginary parts (attributable to small-scale turbulence) about the "mean," which has a constant amplitude but phase varying according to the von Mises pdf. Based on this underlying process, the joint pdfs for the amplitude and phase, and for the real and imaginary parts, were formulated [Eqs. (14) and (15), respectively]. The marginal (single variate) pdf for the amplitude is unchanged by the phase modulation. The marginal pdfs for the phase, and for the real and imaginary parts, are however impacted by the phase modulation. We were unable to derive these marginal pdfs in an analytical form. However, relatively simple one-dimensional integrals were derived, namely, Eq. (17) for the phase distribution, and Eqs. (29) and (30) for the real and imaginary parts. Approaches to approximating the marginal phase distribution with von Mises and wrapped normal distributions were also developed.

While this article focused on phase modulation of the Rice model, an extension to include amplitude modulation could also be useful. Amplitude modulation is produced by turbulent intermittency, i.e., local variations in the intensity of the turbulence. Previously, amplitude modulation of the exponential and Rice pdfs has been used to model intermittency effects.[21,33–36] Furthermore, a recent study showed that amplitude modulation could be incorporated into a gamma distribution (resulting in a compound gamma distribution) to describe propagation uncertainties.[31] In principle, the phase-modulated Rice model could be extended similarly.

ACKNOWLEDGMENTS

This work was supported by the U.S. Army Engineer Research and Development Center, Geospatial Research Engineering basic research program. Permission to publish was granted by the Director, Cold Regions Research and Engineering Laboratory. Any opinions expressed in this paper are those of the authors, and are not to be construed as official positions of the funding agency or the Department of the Army unless so designated by other authorized documents.

APPENDIX: NAKAGAMI AND WRAPPED NORMAL DISTRIBUTIONS

In this Appendix, we examine the suitability of approximating the phase-modulated Rice model with one in which the amplitude fluctuations are modeled with the Nakagami distribution and the phase fluctuations with the wrapped normal distribution.[26] This combination was recently shown to agree well with experimental data for sound propagation in the atmosphere.[26] It can also lead to simpler equations, which enable some analytical results to be obtained in the limit of large phase variance.

The Nakagami pdf is obtained by transforming the gamma pdf for power, Eq. (5), to amplitude $a = s^{1/2}$,

$$f_A(a|k,b) = \frac{2a^{2k-1}}{\Gamma(k)b^k}\exp\left(-\frac{a^2}{b}\right). \tag{A1}$$

01 October 2023 09:00:47

Typically, the Nakagami pdf is parameterized with m and Ω in lieu of k and b, such that $k = m$ and $b = \Omega/m$.[23] Thus

$$f_A(a|m,\Omega) = \frac{2m^m a^{2m-1}}{\Gamma(m)\Omega^m}\exp\left(-\frac{ma^2}{\Omega}\right). \tag{A2}$$

Normalizing the power by its mean, $\Omega = mb = kb = 1$. The pdf for the amplitude then reduces to a single parameter,

$$f_A(a|m) = \frac{2m^m a^{2m-1}}{\Gamma(m)}\exp(-ma^2). \tag{A3}$$

In the following, we will employ the wrapped normal distribution, Eq. (7), but in the form of a Fourier series. Since the distribution is an even function of ϕ, only the cosine terms in ϕ must be retained, i.e.,

$$f_\Phi(\phi) = \frac{a_0}{2} + \sum_{n=1}^{\infty} a_n \cos(n\phi). \tag{A4}$$

Here, the coefficients a_n are given by

$$a_n = \frac{1}{\pi}\int_{-\pi}^{\pi} f_\Phi(\phi)\cos(n\phi)\,d\phi. \tag{A5}$$

The coefficients and circular moments are simply related as $a_n = m_n/\pi$. Thus, for the wrapped normal pdf, $a_n = \exp(-n^2\sigma^2/2)/\pi$ and we have for the phase distribution

$$f_\Phi(\phi) = \frac{1}{2\pi} + \frac{1}{\pi}\sum_{n=1}^{\infty} e^{-n^2\sigma^2/2}\cos(n\phi). \tag{A6}$$

The Fourier series representation is particularly advantageous for large phase variance ($\sigma^2 \gtrsim 1$), in which case only a few terms typically need to be retained. (Note that we are using σ^2 here to indicate the unwrapped phase variance in a normal distribution, whereas in the body of the text we used σ^2 to indicate the variances of the real and imaginary parts in the Rice model.) The first term in Eq. (A6) corresponds to a uniformly distributed phase. Additional terms progressively refine that solution. The following inequality can be used to estimate the error from truncating the Fourier series at the first m terms,

$$\left|\frac{1}{\pi}\sum_{n=m}^{\infty} e^{-n^2\sigma^2/2}\cos(n\phi)\right| < \frac{1}{\sqrt{2\pi}\sigma}\operatorname{erfc}\left(\frac{\sigma(m-1)}{\sqrt{2}}\right). \tag{A7}$$

On the other hand, the wrapped series Eq. (7) is more advantageous when $\sigma^2 \ll 1$, i.e., scattering is weak.

Assuming the amplitude and phase fluctuations are independent, $f_{A\Phi}(a,\phi) = f_A(a)f_\Phi(\phi)$. Using Eq. (A3) for amplitude and the wrapped normal pdf Eq. (A6) for phase, we obtain the joint distribution,

$$f_{A\Phi}(a,\phi) = \frac{2m^m a^{2m-1}}{\pi\Gamma(m)}e^{-ma^2}\left[\frac{1}{2} + \sum_{n=1}^{\infty} e^{-n^2\sigma^2/2}\cos(n\phi)\right]. \tag{A8}$$

The joint pdf of the real x and imaginary y components is then obtained as

$$f_{XY}(x,y) = \frac{2m^m}{\pi\Gamma(m)}\left[\frac{1}{2} + \sum_{n=1}^{\infty} e^{-n^2\sigma^2/2}T_n\left(\frac{x}{\sqrt{x^2+y^2}}\right)\right] \times (x^2+y^2)^{m-1}e^{-m(x^2+y^2)}, \tag{A9}$$

where we have used the relationships $\cos\phi = x/\sqrt{x^2+y^2}$ and $T_n(\cos\phi) = \cos(n\phi)$, with T_n being the Chebyshev polynomial of the first kind. General analytical solutions for the marginal pdfs $f_X(x)$ and $f_Y(y)$ do not appear to be obtainable from Eq. (A9). However, Eq. (A9) provides a very convenient solution from a numerical perspective: one must only evaluate $f_{XY}(x,y)$ on a grid of points in x and y and then apply a numerical integration over one of these variables. The Chebyshev series typically converges quickly.

The marginal pdfs implied Eq. (A9) are not independent. The condition $f_{XY}(x,y) = f_X(x)f_Y(y)$ is met only when $m = 1$ and $\sigma^2 \to \infty$, which corresponds to full saturation. In this case, the sum over n is zero, and the integrals in Eqs. (27) and (28) evaluate to $f_X(x) = (1/\sqrt{\pi})e^{-x^2}$ and $f_Y(y) = (1/\sqrt{\pi})e^{-y^2}$. These are normal pdfs with a variance of 1/2. This outcome is to be expected, because in full saturation the mean power is the sum of the variances of the real and imaginary parts, and the mean power has been normalized to one.

Nonetheless, some progress towards analytical solutions can be made for large phase variance (i.e., $\sigma^2 \gtrsim 1$). To start, substitute Eq. (A9) into Eq. (27) and take into account that the integrand is an even function of y,

$$f_X(x) = \frac{2m^m e^{-mx^2}}{\pi\Gamma(m)}\int_0^\infty\left[1 + 2\sum_{n=1}^{\infty} e^{-n^2\sigma^2/2}T_n\left(\frac{x}{\sqrt{x^2+y^2}}\right)\right] \times (x^2+y^2)^{m-1}e^{-my^2}\,dy. \tag{A10}$$

Next, make the substitution $\eta = y/|x|$, followed by $\xi = \eta^2$. The result is

$$f_X(x) = \frac{m^m|x|^{2m-1}e^{-mx^2}}{\pi\Gamma(m)}\int_0^\infty\left[1 + 2\sum_{n=1}^{\infty} e^{-n^2\sigma^2/2}T_n\left(\frac{\operatorname{sgn}(x)}{\sqrt{1+\xi}}\right)\right] \times \xi^{-1/2}(1+\xi)^{m-1}e^{-mx^2\xi}\,d\xi, \tag{A11}$$

where $\operatorname{sgn}(x) = -1$ when $x < 0$ and $+1$ otherwise. For arbitrary m and large σ^2, the sum in Eq. (A11) may be terminated after a small number of terms. Keeping the first four terms, and taking into account that $T_0(z) = 1$, $T_1(z) = z$, $T_2(z) = 2z^2 - 1$, $T_3(z) = 4z^3 - 3z$, and $T_4(z) = 8z^4 - 8z^2 + 1$, we have

$$f_X(x) = \frac{m^m|x|^{2m-1}e^{-mx^2}}{\pi\Gamma(m)}\int_0^\infty\left[1 - 2e^{-2\sigma^2} + 2e^{-8\sigma^2} + \frac{2\operatorname{sgn}(x)(e^{-\sigma^2/2} - 3e^{-9\sigma^2/2})}{(1+\xi)^{1/2}} + \frac{4(e^{-2\sigma^2} - 4e^{-8\sigma^2})}{1+\xi} + \frac{8\operatorname{sgn}(x)e^{-9\sigma^2/2}}{(1+\xi)^{3/2}} + \frac{16e^{-8\sigma^2}}{(1+\xi)^2}\right] \times \xi^{-1/2}(1+\xi)^{m-1}e^{-mx^2\xi}\,d\xi. \tag{A12}$$

01 October 2023 09:00:47

On the right-hand side of this formula, the integrals can be expressed in terms of the confluent hypergeometric function of the second kind, $U(a,b,z)$, which in integral form is

$$U(a,b,z)=\frac{1}{\Gamma(a)}\int_0^\infty t^{a-1}(1+t)^{b-a-1}e^{-zt}\,dt. \tag{A13}$$

Hence, we have the result

$$\begin{aligned} f_X(x)=&\frac{m^m|x|^{2m-1}e^{-mx^2}}{\sqrt{\pi}\Gamma(m)}\Bigg[\left(1-2e^{-2\sigma^2}+2e^{-8\sigma^2}\right)\\ &\times U\left(\frac{1}{2},m+\frac{1}{2},mx^2\right)+2\mathrm{sgn}(x)\left(e^{-\sigma^2/2}-3e^{-9\sigma^2/2}\right)\\ &\times U\left(\frac{1}{2},m,mx^2\right)+4\left(e^{-2\sigma^2}-4e^{-8\sigma^2}\right)\\ &\times U\left(\frac{1}{2},m-\frac{1}{2},mx^2\right)+8\mathrm{sgn}(x)e^{-9\sigma^2/2}\\ &\times U\left(\frac{1}{2},m-1,mx^2\right)+16e^{-8\sigma^2}U\left(\frac{1}{2},m-\frac{3}{2},mx^2\right)\Bigg]. \end{aligned} \tag{A14}$$

In Figs. 10 and 11, the pdfs for the real component of the complex signal predicted by the Nakagami/wrapped normal model are compared to predictions from the phase-modulated Rice model. The first figure is for a Rice factor $K=1$ and the second for $K=4$. The unwrapped phase variances in the wrapped normal pdf (σ^2) are chosen to match the circular variances for the corresponding Rice factors as described in the body of the text. The dashed lines in the figures correspond to Eq. (A9) after numerically integrating over y. The circles are the analytical approximation to the Nakagami/wrapped normal model given by Eq. (A14). We see that, except for the largest values of K and κ plotted (4 and 16, respectively), Eq. (A14) is essentially indistinguishable from the more exact result obtained by integrating Eq. (A9). On the other hand, some discrepancies between the Nakagami/wrapped normal model and the phase-modulated Rice model are evident.

The distribution for the imaginary component is obtained by substituting Eq. (A9) into Eq. (28) with the result

$$\begin{aligned} f_Y(y)=&\frac{2m^m e^{-my^2}}{\pi\Gamma(m)}\int_{-\infty}^{\infty}\left[\frac{1}{2}+\sum_{n=1}^{\infty}e^{-n^2\sigma^2/2}T_n\left(\frac{x}{\sqrt{x^2+y^2}}\right)\right]\\ &\times\left(x^2+y^2\right)^{m-1}e^{-mx^2}\,dx. \end{aligned} \tag{A15}$$

Here, the integrand is an even function of x when n is even and an odd function when n is odd. Therefore, in Eq. (A15) all integrals corresponding to odd n are zero and this equation can be written as

$$\begin{aligned} f_Y(y)=&\frac{2m^m e^{-my^2}}{\pi\Gamma(m)}\int_{0}^{\infty}\left[1+2\sum_{n=1}^{\infty}e^{-(2n)^2\sigma^2/2}T_{2n}\left(\frac{x}{\sqrt{x^2+y^2}}\right)\right]\\ &\times\left(x^2+y^2\right)^{m-1}e^{-mx^2}\,dx. \end{aligned} \tag{A16}$$

Next, we make the substitution $\eta=x/|y|$, followed by $\xi=\eta^2$, with result

$$\begin{aligned} f_Y(y)=&\frac{m^m|y|^{2m-1}e^{-my^2}}{\pi\Gamma(m)}\\ &\times\int_0^\infty\left[1+2\sum_{n=1}^{\infty}e^{-(2n)^2\sigma^2/2}T_{2n}\left(\sqrt{\frac{\xi}{1+\xi}}\right)\right]\\ &\times\xi^{-1/2}(1+\xi)^{m-1}e^{-my^2\xi}\,d\xi. \end{aligned} \tag{A17}$$

Analyzing the imaginary part in the same manner as the real part, we arrive at

$$\begin{aligned} f_Y(y)=&\frac{m^m y^{2m-1}e^{-my^2}}{\sqrt{\pi}\Gamma(m)}\Bigg[\left(1-2e^{-2\sigma^2}\right)U\left(\frac{1}{2},m+\frac{1}{2},my^2\right)\\ &+2e^{-2\sigma^2}U\left(\frac{3}{2},m+\frac{1}{2},my^2\right)\\ &+12e^{-8\sigma^2}U\left(\frac{5}{2},m-\frac{3}{2},my^2\right)-8e^{-8\sigma^2}U\left(\frac{3}{2},m-\frac{1}{2},my^2\right)\\ &+2e^{-8\sigma^2}U\left(\frac{1}{2},m+\frac{1}{2},my^2\right)\Bigg]. \end{aligned} \tag{A18}$$

Figures 12 and 13 show the pdfs for the imaginary component predicted by the Nakagami/wrapped normal model and compare them to predictions from the phase-modulated Rice model. As with the real component (Figs. 10 and 11), Eq. (A18) provides an excellent approximation for the Nakagami/wrapped normal model, although this model differs noticeably from the phase-modulated Rice model.

[1]V. E. Ostashev and D. K. Wilson, *Acoustics in Moving Inhomogeneous Media*, 2nd ed. (CRC Press, Boca Raton, FL, 2015), p. 521.
[2]D. K. Wilson, C. L. Pettit, and V. E. Ostashev, "Sound propagation in the atmospheric boundary layer," Acoust. Today **11**, 44–53 (2015).
[3]F. Rietdijk, J. Forssén, and K. Heutschi, "Generating sequences of acoustic scintillations," Acta Acust. united Ac. **103**(2), 331–338 (2017).
[4]D. K. Wilson, V. E. Ostashev, and C. L. Pettit, "Distribution of the two-point product of complex amplitudes in the fully saturated scattering regime," J. Acoust. Soc. Am. **148**(4), EL347–EL352 (2020).
[5]C. Dreier and M. Vorländer, "Aircraft noise—Auralization-based assessment of weather-dependent effects on loudness and sharpness," J. Acoust. Soc. Am. **149**(5), 3565–3575 (2021).
[6]D. K. Wilson, M. J. Kamrath, C. E. Haedrich, D. J. Breton, and C. R. Hart, "Urban noise distributions and the influence of geometric spreading on skewness," J. Acoust. Soc. Am. **150**(2), 783–800 (2021).
[7]S. M. Rytov, Y. A. Kravtsov, and V. I. Tatarskii, *Principles of Statistical Radio Physics* (Springer, Berlin, 1989).
[8]H. Suzuki, "A statistical model for urban radio propagation," IEEE Trans. Commun. **25**(7), 673–680 (1977).
[9]D. J. Breton, C. E. Haedrich, M. J. Kamrath, and D. K. Wilson, "Street-scale mapping of urban radio frequency noise at very high frequency and ultra high frequency," Radio Sci. **54**(11), 934–948, https://doi.org/10.1029/2019RS006893 (2019).
[10]J. W. Strohbehn, T. Wang, and J. P. Speck, "On the probability distribution of line-of-sight fluctuations of optical signals," Radio Sci. **10**(1), 59–70, https://doi.org/10.1029/RS010i001p00059 (1975).
[11]L. C. Andrews and R. L. Phillips, *Laser Beam Propagation through Random Media* (SPIE, Bellingham, WA, 2005), p. 808.
[12]W. S. Burdic, *Underwater Acoustic System Analysis* (Prentice Hall, Englewood Cliffs, NJ, 1991), p. 320.

01 October 2023 09:00:47

[13]R. Dashen, W. H. Munk, K. M. Watson, and F. Zachariasen, and S. M. Flatte, *Sound Transmission through a Fluctuating Ocean* (Cambridge University Press, New York, 1979), p. 290.
[14]T. E. Ewart and D. B. Percival, "Forward scattered waves in random media—The probability distribution of intensity," J. Acoust. Soc. Am. **80**(6), 1745–1753 (1986).
[15]D. E. Norris, D. K. Wilson, and D. W. Thomson, "Correlations between acoustic travel-time fluctuations and turbulence in the atmospheric surface layer," Acta Acust. united Ac. **87**(6), 677–684 (2001).
[16]S. Cheinet, M. Cosnefroy, F. Königstein, W. Rickert, M. Christoph, S. L. Collier, A. Dagallier, L. Ehrhardt, V. E. Ostashev, A. Stefanovic, T. Wessling, and D. K. Wilson, "An experimental study of the atmospheric-driven variability of impulse sounds," J. Acoust. Soc. Am. **144**(2), 822–840 (2018).
[17]M. J. Kamrath, V. E. Ostashev, D. K. Wilson, M. J. White, C. R. Hart, and A. Finn, "Vertical and slanted sound propagation in the near-ground atmosphere: Amplitude and phase fluctuations," J. Acoust. Soc. Am. **149**(3), 2055–2071 (2021).
[18]V. E. Ostashev, M. J. Kamrath, D. K. Wilson, M. J. White, C. R. Hart, and A. Finn, "Vertical and slanted sound propagation in the near-ground atmosphere: Coherence and distributions," J. Acoust. Soc. Am. **150**(4), 3109–3126 (2021).
[19]S. O. Rice, "Mathematical analysis of random noise," Bell Syst. Technol. J. **24**, 46–156 (1945).
[20]V. P. Mamyshev and S. L. Odintsov, "Phase variance of narrow-band acoustic signals on near-surface paths," Atmos. Oceanic Opt. **30**(3), 236–242 (2017).
[21]D. E. Norris, D. K. Wilson, and D. W. Thomson, "Atmospheric scattering for varying degrees of saturation and turbulent intermittency," J. Acoust. Soc. Am. **109**(5), 1871–1880 (2001).
[22]I. S. Gradshteyn and I. M. Ryzhik, *Table of Integrals, Series, and Products* (Academic Press, New York, 2014), p. 1220.
[23]M. Nakagami, "The m-Distribution—A general formula of intensity of rapid fading," in *Statistical Methods in Radio Wave Propagation*, edited by W. C. Hoffman (Pergamon, Oxford, UK, 1960), pp. 3–36.
[24]Z. Luo, Y. Zhan, and E. Jonckheere, "Analysis of functions and characteristics of the Rician phase distribution," in *Proceedings of the IEEE/CIC International Conference on Communications in China (ICCC)*, Virtual (August 9–11, 2020).
[25]F. Pfaff, G. Kurz, and U. D. Hanebeck, "Multimodal circular filtering using Fourier series," in *Proceedings of the 18th International Conference on Information Fusion*, Washington, DC (July 6–9, 2015), pp. 711–718.
[26]M. J. Kamrath, "Evaluation of a gamma power, wrapped normal phase model for vertical and slanted atmospheric sound propagation," J. Acoust. Soc. Am. **152**, A57 (2022).
[27]C. Tellambura and A. D. S. Jayalath, "Generation of bivariate Rayleigh and Nakagami-m fading envelopes," IEEE Commun. Lett. **4**(5), 170–172 (2000).
[28]D. B. da Costa and M. D. Yacoub, "The η-μ joint phase-envelope distribution," IEEE Antennas Wirel. Propag. Lett. **6**, 195–198 (2007).
[29]V. E. Ostashev and D. K. Wilson, "Strength and wave parameters for sound propagation in random media," J. Acoust. Soc. Am. **141**(3), 2079–2092 (2017).
[30]M. West, K. Gilbert, and R. A. Sack, "A tutorial on the parabolic equation (PE) model used for long range sound propagation in the atmosphere," Appl. Acoust. **37**, 31–49 (1992).
[31]D. K. Wilson, C. L. Pettit, V. E. Ostashev, and M. J. Kamrath, "Signal power distributions for simulated outdoor sound propagation in varying refractive conditions," J. Acoust. Soc. Am. **151**(6), 3895–3906 (2022).
[32]S. Kullback and R. A. Leibler, "On information and sufficiency," Ann. Math. Statist. **22**, 79–86 (1951).
[33]A. S. Gurvich and V. P. Kukharets, "The influence of intermittence of atmospheric turbulence on the scattering of radio waves," Sov. J. Commun. Technol. Electron. **30**, 52–58 (1986).
[34]J. H. Churnside and S. F. Clifford, "Log-normal Rician probability-density function of optical scintillations in the turbulent atmosphere," J. Opt. Soc. Am. A **4**(10), 1923–1930 (1987).
[35]J. H. Churnside, "Joint probability-density function of irradiance scintillations in the turbulent atmosphere," J. Opt. Soc. Am. A **6**(12), 1931–1940 (1989).
[36]D. K. Wilson, J. C. Wyngaard, and D. I. Havelock, "The effect of turbulent intermittency on scattering into an acoustic shadow zone," J. Acoust. Soc. Am. **99**(6), 3393–3400 (1996).

01 October 2023 09:00:47